



A sulfonamidoquinoline-derived Zn²⁺ fluorescent sensor with 1:1 Zn²⁺ binding stoichiometry

Changli Zhang^{a,b}, Yuming Zhang^{a,c}, Yuncong Chen^a, Zhijun Xie^a, Zhipeng Liu^a, Xindian Dong^a, Weijiang He^{a,*}, Chen Shen^a, Zijian Guo^{a,*}

^a State Key Laboratory of Coordination Chemistry, Coordination Chemistry Institute, School of Chemistry and Chemical Engineering, Nanjing University, Nanjing 210093, PR China

^b Department of Chemistry, Nanjing Xiaozhuang College, Nanjing 210017, PR China

^c Xingling College, Nantong University, Nantong 226009, PR China

ARTICLE INFO

Article history:

Received 1 October 2010

Accepted 17 November 2010

Available online 25 November 2010

Keywords:

Sulfonamidoquinoline

Zinc

Fluorescent sensor

Imaging

ABSTRACT

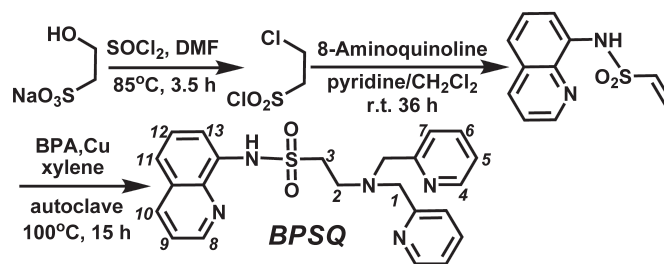
The integration of bis(pyridin-2-ylmethyl)amine (BPA) with 8-sulfonamidoquinoline (SQ) resulted in a new fluorescent Zn²⁺ sensor of 1:1 binding stoichiometry. The synergic Zn²⁺ coordination of BPA and SQ motifs provides the sensor the advantage over TSQ and its analogues in discriminating mobile Zn²⁺ from the bound Zn²⁺ of unoccupied coordination sites in living systems. Its pH-independent Zn²⁺-enhanced emission in physiological condition and cell permeability make it an effective intracellular Zn²⁺ imaging agent. This sensor profits also from its confirmed Golgi-preferential affinity, and its pH-independent Zn²⁺ response in physiological pH range provides it the advantages over other xanthenone-based sensors.

© 2010 Elsevier B.V. All rights reserved.

Mobile Zn²⁺ is an important transmitter in neural signal transmission, and is also proposed to regulate the pathophysiology of many severe neurological diseases [1]. Mobile Zn²⁺ is also involved in the signal transduction process [2]. The spatial and temporal Zn²⁺ tracking via fluorescent sensor staining is of great significance for clarifying the mobile Zn²⁺-involved physiological process [1,3]. TSQ (6-methoxy-(8-*p*-toluene sulfonamido)quinoline) and its analogue Zinquin have been widely adopted to image mobile Zn²⁺ in cells and tissues [4]. These classical Zn²⁺ fluorescence sensors exhibit the distinct Zn²⁺-triggered “turn-on” fluorescence, cell permeability and favorable pH-independence emission. Although many Zn²⁺ fluorescent sensors have been reported [5], the diversified microenvironments in living systems demand sensors of different properties, and modification of 8-sulfonamidoquinoline (SQ) is still an attractive strategy [6]. However, the reported SQ-derived sensors are difficult in discriminating mobile Zn²⁺ from the bound Zn²⁺ of unoccupied coordination sites in living systems, since these bidentates require extra ligand to stabilize their Zn²⁺ complexes [5,6]. In fact, their Zn²⁺ binding stoichiometry is 2:1 (Sensor/Zn²⁺). Modifying SQ-derived sensors with additional synergic Zn²⁺ coordination sites to acquire 1:1 Zn²⁺ binding stoichiometry should be helpful to overcome this disadvantage. In this study, a new Zn²⁺ fluorescent sensor, BPSQ, was constructed for this purpose by combining SQ with the synergic zinc coordinating motif, bis(pyridin-2-ylmethyl)amine (BPA) (Scheme 1).

The spectroscopic study of BPSQ was investigated in HEPES buffer (pH, 7.2) containing 5% DMSO except for the pH titration. BPSQ (10 μM) exhibits an intensive absorption band centered at 302 nm (Fig. 1a). Zn²⁺ titration demonstrates the linear decrease of this band and linear increase of a new band centered at 360 nm, when the [Zn²⁺]_{total}/[BPSQ] ratio being lower than 1:1. The stable spectra thereafter and the clear isosbestic point at 326 nm suggest that only one Zn²⁺ complex species is formed. The titration profiles according to the absorbance at 302 and 360 nm suggest this complex possess the Zn²⁺ binding stoichiometry of 1:1.

BPSQ in HEPES buffer exhibits a typical broad emission band of TSQ and analogues, centering at 532 nm with a shoulder peak at 497 nm (λ_{ex}, 364 nm). The pH titration demonstrates the stable emission from pH 6.0 to 10.0, which makes BPSQ suitable for application in physiological condition (Fig. S6). However, the higher pH above 10 leads to the distinct emission enhancement, suggesting the



Scheme 1. Synthesis of BPSQ.

* Corresponding authors. Fax: +86 25 83314502.

E-mail addresses: hewej69@nju.edu.cn (W. He), zguo@nju.edu.cn (Z. Guo).

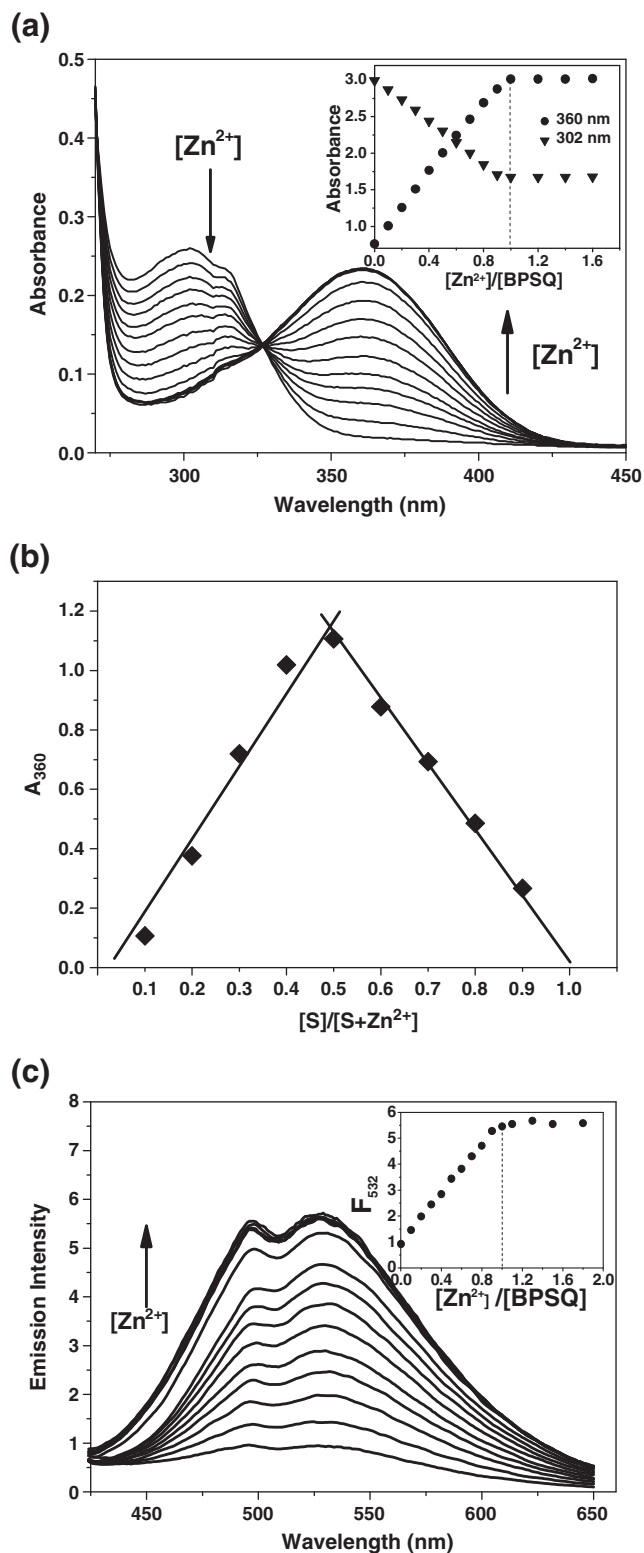


Fig. 1. (a) Absorption spectra of BPSQ (50 μM) in HEPES buffer (50 mM, 0.1 M KNO_3 , pH, 7.2, 5% DMSO) when titrated by Zn^{2+} . Inset, the titration profiles based on A_{302} and A_{360} . (b) Job's plot of BPSQ and Zn^{2+} in the same medium according to the absorbance at 360 nm. The total concentration of Zn^{2+} and BPSQ is 0.5 mM. S, BPSQ. (c) Emission spectra of BPSQ (5 μM) in the same medium when titrated by Zn^{2+} . Inset, the titration profiles based on F_{532} . λ_{exc} , 364 nm. $[\text{Zn}^{2+}]_{\text{total}}$ increases along the direction of the arrow.

sulfonamide deprotonation favor the enhancement ($pK_{a1} \sim 10.8$). Decreasing pH from 6.0 to 3.0 also results in the emission enhancement due to PET blockage ($pK_{a2} \sim 4.4$). Zn^{2+} titration of

BPSQ displays the distinct linear emission enhancement (Fig. 1b), and the emission become stable when the $[\text{Zn}^{2+}]_{\text{total}}/[\text{BPSQ}]$ ratio being higher than 1:1. The dissociation constant (K_d) of $\text{Zn}^{2+}/\text{BPSQ}$ complex was determined to be $(1.8 \pm 0.1) \times 10^{-12}$ M via fluorescence titration in a series of Zn^{2+} buffer [7]. The limit of detection (LOD) for Zn^{2+} is $\sim 4.2 \times 10^{-14}$ M ($3\sigma/\text{slope}$, see supporting information). The quantum yield of BPSQ and its Zn^{2+} complex is determined as 0.015 (ϵ_{364} , 420 $\text{M}^{-1} \text{cm}^{-1}$) and 0.055 (ϵ_{364} , 4680 $\text{M}^{-1} \text{cm}^{-1}$) with quinine sulfate solution ($\Phi = 0.546$, 0.5 M H_2SO_4) as reference. On the other hand, single crystal structural analysis of its zinc complex exhibits a 1:1 Zn^{2+} binding stoichiometry of BPSQ. In this complex, Zn^{2+} center adopts a distorted octahedral geometry with three BPA N atoms and one quinoline N atom occupying the equatorial plane vertexes. The two axial sites are occupied by the sulfonamide N atom and a water O atom. The quinoline plane is almost perpendicular to the BPA pyridine planes (Fig. 2). Structural analysis demonstrates the direct Zn^{2+} coordination of sulfonamide N via deprotonation. In addition, ^1H NMR Zn^{2+} titration of BPSQ displays the distinct changes in spectrum upon Zn^{2+} addition, and the spectrum becomes stable when $[\text{Zn}^{2+}]/[\text{BPSQ}]$ being higher than 1:1 (Fig. S9). The signal of H8 undergoes a distinct downfield shift from 8.77 to 9.06 ppm upon Zn^{2+} addition, implying that the quinoline N should be involved directly in Zn^{2+} coordination. In addition, this coordination still induces the signal shifts of other protons from the N-containing ring of quinoline. The Zn^{2+} coordination-induced sulfonamide deprotonation induces also the signal shift of protons from another quinoline ring. Zn^{2+} coordination to BPA motif in solution has also been confirmed by the ^1H NMR monitoring (Table S3, Fig. S9). ^1H NMR titration suggests that the solution coordination structure is almost identical to the crystal structure. Therefore, the Zn^{2+} -induced emission enhancement should have the similar origin of other SQ-based Zn^{2+} sensors: Zn^{2+} coordination to sulfonamide and quinoline N atom [6]. In addition, the PET (photo-induced electron transfer) blockage via outer amine Zn^{2+} coordination may also induce the enhanced emission [3].

Cation-induced changes in emission enhancement factor F/F_0 at 532 nm were investigated to determine the specific Zn^{2+} sensing ability of BPSQ. Zn^{2+} and Cd^{2+} (1 equiv) induce F/F_0 increase from 1 to 9.3 and 9.0, respectively. Considering the scarcity of Cd^{2+} in living cells, the Cd^{2+} response should not interfere with intracellular Zn^{2+} detection. All other transition metal cations do not lead to any obvious emission enhancement. Although the pretreatment by Co^{2+} , Cu^{2+} ,

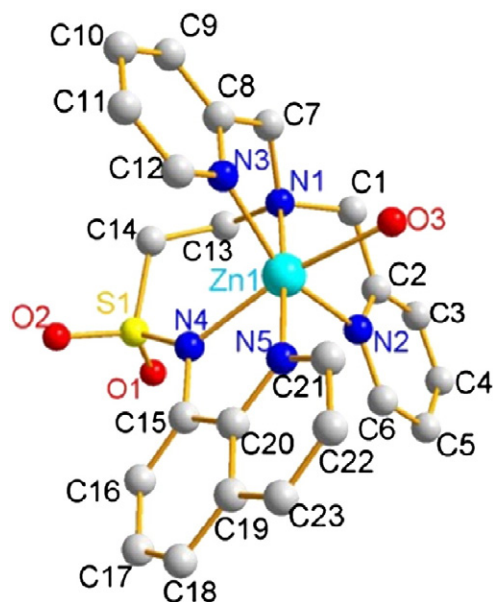


Fig. 2. Structural diagram of $[\text{Zn}(\text{BPSQ-H})(\text{H}_2\text{O})]\text{NO}_3$. The protons and anion are omitted for clarification.

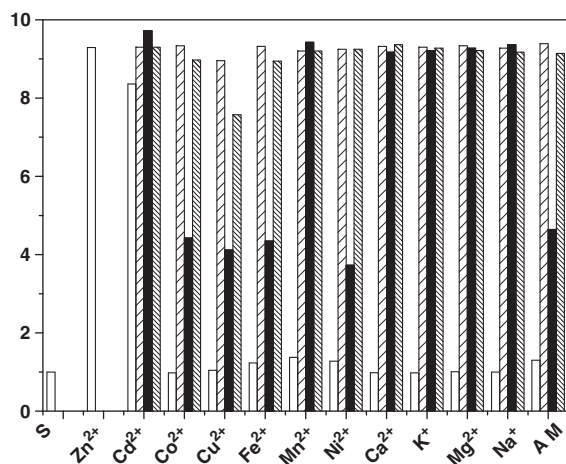


Fig. 3. Emission enhancement factor (F/F_0 at 532 nm) of BPSQ (5 μM) in HEPES buffer (50 mM, 0.1 M KNO_3 , pH, 7.2, 5% DMSO) induced by 1 equiv Zn^{2+} , Cd^{2+} , Co^{2+} , Cu^{2+} , Fe^{2+} , Mn^{2+} and Ni^{2+} and 1000 equiv alkaline/alkaline earth metal cations. None-filled bar, 1 equiv marked cation was added; sparsely-filled bar, the marked cation was added after 1 equiv Zn^{2+} ; black bar, the marked cation was added before 1 equiv Zn^{2+} ; densely-filled bar, the marked cation and Zn^{2+} was added simultaneously. AM: all metal cations including all the tested alkaline/alkaline earth metal cations (1000 equiv each) and transition metal cations (1 equiv each) except Zn^{2+} . S, BPSQ.

Fe^{2+} and Ni^{2+} (1 equiv) decreases the Zn^{2+} -induced enhancement factor from ~ 9.3 to ~ 4.0 , the simultaneous addition of Zn^{2+} and all other metal cations does not decrease this factor evidently (Fig. 3). Moreover, the presence of 1000 equiv of Na^+ , K^+ , Ca^{2+} or Mg^{2+} , which are abundant in cells, does not affect the Zn^{2+} sensing behavior of BPSQ. On the other hand, the fluorescent Zn^{2+} sensing behavior of BPSQ is not affected by different counter anions such as ClO_4^- , Cl^- , NO_3^- , SO_4^{2-} , and CH_3CO_2^- . All these suggest that BPSQ is a suitable candidate for intracellular Zn^{2+} -staining.

The intracellular Zn^{2+} imaging ability of BPSQ has been verified on HeLa cells by confocal imaging. The imaging result discloses that the stained HeLa cells exhibit dim inhomogeneous fluorescence (Fig. 4b). When exogenous Zn^{2+} is introduced by incubation with 5 μM pyrithione/ ZnSO_4 , the cells display the bright punctated fluorescence (Fig. 4c). The following deprivation of the exogenous Zn^{2+} by cell

permeable chelator, *N,N,N',N'*-tetrakis(2-pyridylmethyl)ethylene diamine (TPEN) leads to the dim fluorescence (Fig. 4d). The mean fluorescence intensity of three arbitrarily selected regions in nucleolus (yellow panes) in Fig. 4b, c and d is 13, 118 and 25, respectively. For the selected regions in cytoplasm (red panes), the mean intensity in Fig. 4b, c and d is 8, 40 and 22. The preferential affinity of BPSQ to certain organelles is also observed. Localization studies exhibit that there is no colocalization when lysosome marker Red DND-99 is costained by BPSQ (Fig. 4f). Partial colocalization (in yellow) is observed when mitochondria marker Red CMXRos is costained by BPSQ (Fig. 4g). There is still bright fluorescence (in green) of BPSQ that is not overlaid. The further costaining experiment with Golgi marker BODIPY TR Ceramide indicates that Golgi is the main preferential organelle for BPSQ (Fig. 4h).

In conclusion, the newly developed Zn^{2+} fluorescent sensor BPSQ displays not only the specific Zn^{2+} -induced fluorescence response in aqueous media, but also the 1:1 Zn^{2+} binding stoichiometry. This stoichiometry provides this SQ-based sensor the ability to reduce the interference in labile Zn^{2+} detection induced by the bound Zn^{2+} of unoccupied coordination sites. The pH-independent fluorescence in physiological condition, high Zn^{2+} selectivity/sensitivity and its cell membrane permeability make this sensor an effective intracellular Zn^{2+} imaging agent. Moreover, the current result displays a successful modification of classic Zn^{2+} sensor as a new sensor of improved imaging ability.

Acknowledgements

We thank the National Science Foundation of China (Nos. 20871066, 20631020, 90713001 20721002 and 10979019), National Basic Research Program of China (No. 2011CB935800) and the Natural Science Foundation of Jiangsu (BK2008015 and BK2009227) for the financial support.

Appendix A. Supplementary material

Supplementary data to this article can be found online at doi:10.1016/j.inoche.2010.11.021.

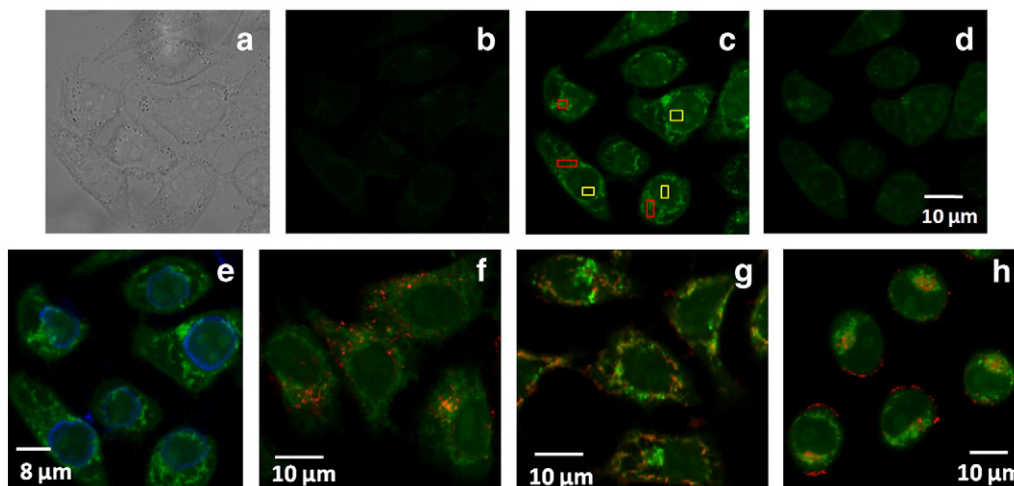


Fig. 4. (a) Confocal microscopic images of HeLa cells stained by BPSQ (10 μM , 1 \times PBS, 20 min of incubation). λ_{ex} , 405 nm. (b–d), fluorescence images via single channel imaging (410–570 nm). (a), Bright-field transmission images; (b) images of BPSQ-stained cells; (c) fluorescence images of the rinsed cells in (b) followed by incubation with pyrithione/ ZnSO_4 (1:1, 5 μM , 5 min) and BPSQ (10 μM , 20 min) in sequence; (d) fluorescence image of the cells in (c) followed by treatment with 50 μM TPEN (5 min). (e–h) Colocalization images of cells incubated with 5 μM pyrithione/ ZnSO_4 (1:1) solution (5 μM , 5 min) followed by costaining with BPSQ and organelle dye. Image of cells stained by Hoechst 33342 (5 μM , 15 min) and BPSQ (e), by LysoTracker Red DND-99 (50 nM, 15 min) and BPSQ (f), by MitoTracker Red CMXRos (50 nM, 15 min) and BPSQ (g), by Golgi marker BODIPY TR Ceramide (5 μM , 30 min, 4 $^\circ\text{C}$) and BPSQ (h).

References

- [1] (a) L.A. Finney, T.V. O'Halloran, *Science* 300 (2003) 931;
(b) A.C. Burdette, S.J. Lippard, *Proc. Natl. Acad. Sci. USA* 100 (2003) 3605;
(c) D.W. Choi, J.Y. Koh, *Ann. Rev. Neurosci.* 21 (1998) 347.
- [2] (a) D.H. Nies, *Science* 317 (2007) 1695;
(b) M. Lu, D. Fu, *Science* 317 (2007) 1746.
- [3] (a) P. Jiang, Z. Guo, *Coord. Chem. Rev.* 248 (2004) 205;
(b) D.W. Domaille, E.L. Que, C.J. Chang, *Nat. Chem. Biol.* 4 (2008) 168;
(c) P. Carol, S. Sreejith, A. Ajayaghosh, *Chem. Asian J.* 2 (2007) 338;
(d) K. Kikuchi, K. Komatsu, T. Nagano, *Curr. Opin. Chem. Biol.* 8 (2004) 182.
- [4] (a) C.J. Frederickson, E.J. Kasarskis, D. Ringo, R.E. Frederickson, *J. Neurosci. Methods* 20 (1987) 91;
(b) D. Savage, C.Y. Montano, E.J. Kasarkis, *Brain Res.* 496 (1989) 257;
(c) P.D. Zalewski, J. Forbes, R.F. Seemark, R. Borlinghaus, W.H. Betts, S.F. Lincoln, A.D. Ward, *Chem. Biol.* 1 (1994) 153;
(d) I.B. Mahadevan, M.C. Kimber, S.F. Lincoln, E.R.T. Tiekink, A.D. Ward, W.H. Betts, I.J. Forbes, P.D. Zalewski, *Aust. J. Chem.* 49 (1996) 561.
- [5] (a) G.K. Walkup, S.C. Burdette, S.J. Lippard, R.Y. Tsien, *J. Am. Chem. Soc.* 122 (2000) 5644;
(b) K. Komatsu, K. Kikuchi, H. Kojima, Y. Urano, T. Nagano, *J. Am. Chem. Soc.* 127 (2005) 10197;
(c) A. Ajayaghosh, P. Carol, S. Sreejith, *J. Am. Chem. Soc.* 127 (2005) 14962;
(d) M.M. Henary, Y. Wu, C.J. Fahrni, *Chem. Eur. J.* 10 (2004) 3015;
(e) N.C. Lim, J.V. Schuster, M.C. Porto, M.A. Tanudra, L.L. Yao, H.C. Freake, C. Brückner, *Inorg. Chem.* 44 (2005) 2018;
(f) E. Tamanini, A. Katewa, L.M. Sedger, M.H. Todd, M. Watkinson, *Inorg. Chem.* 48 (2009) 319;
(g) F. Qian, C. Zhang, Y. Zhang, W. He, X. Gao, P. Hu, Z. Guo, *J. Am. Chem. Soc.* 131 (2009) 1460;
(h) H.M. Kim, M.S. Seo, M.J. An, J.H. Hong, Y.S. Tian, J.H. Choi, O. Kwon, K.J. Lee, B.R. Cho, *Angew. Chem. Int. Ed.* 47 (2008) 5167.
- [6] (a) M.S. Nasir, C.J. Fahrni, D.A. Suhy, K.J. Kolodnick, C.P. Singer, T.V. O'Halloran, *J. Biol. Inorg. Chem.* 4 (1999) 775;
(b) C.J. Fahrni, T.V. O'Halloran, *J. Am. Chem. Soc.* 121 (1999) 11448;
(c) M.C. Kimber, I.B. Mahadevan, S.F. Lincoln, A.D. Ward, W.H. Betts, *Aust. J. Chem.* 54 (2001) 43;
(d) G. Xue, J.S. Bradshaw, N.K. Dalley, P.B. Savage, R.M. Izatt, L. Prodi, M. Montalti, N. Zaccaroni, *Tetrahedron* 58 (2002) 4809;
(e) P. Jiang, L. Chen, J. Lin, Q. Liu, J. Ding, X. Gao, Z. Guo, *Chem. Commun.* (2002) 1424;
(f) P. Teolato, E. Rampazzo, M. Arduini, F. Mancin, P. Tecilla, U. Tonellato, *Chem. Eur. J.* 13 (2007) 2238;
(g) N. Zhang, Y. Chen, M. Yu, Y. Liu, *Chem. Asian J.* 4 (2009) 1697;
(h) H.-H. Wang, Q. Gan, X.-J. Wang, L. Xue, S.-H. Liu, H. Jiang, *Org. Lett.* 9 (2007) 4995;
(i) L. Canovese, F. Visentin, G. Chessa, C. Levi, A. Dolmella, *Eur. J. Inorg. Chem.* (2007) 3669.
- [7] M. Taki, J.L. Wolford, T.V. O'Halloran, *J. Am. Chem. Soc.* 126 (2004) 712.